Ubiquitin proteomics reveals critical targets of the Nse1 RING domain in rDNA and genome stability

Eva Ibars[1], Gemma Bellí[1], Celia Casas[1], Joan Codina-Fabra[1], Marc Tarrés[1], Roger Solé-Soler[1], Pilar Ximénez-Embún[2], Javier Muñoz[2,3], Neus Colomina[1], Jordi Torres-Rosell[1*]

[1] Departament de Ciencies Mediques Basiques, Institut de Recerca Biomedica de Lleida, Universitat de Lleida, 25198 Lleida, Spain

[2] Proteomics Unit. Spanish National Cancer Research Center (CNIO), Madrid, Spain; ProteoRed-ISCIII. Madrid, Spain

[3] Present address: Biocruces Bizkaia Health Research Institute, Barakaldo, Spain; Ikerbasque, Basque Foundation for Science. Bilbao, Spain

* Correspondence: jordi.torres@udl.cat

Lead Contact: Jordi Torres-Rosell

ABSTRACT

Ubiquitination controls numerous cellular processes, and its deregulation is associated to many pathologies. The Nse1 subunit in the Smc5/6 complex contains a RING domain with ubiquitin E3 ligase activity and important functions in genome integrity. However, Nse1-dependent ubiquitin targets remain largely unknown. Here, we use label-free quantitative proteomics to analyse the nuclear ubiquitinome of *nse1-C274A* RING mutant cells. Our results show that Nse1 impacts on the ubiquitination of several proteins involved in DNA damage tolerance, ribosome biogenesis and metabolism that, importantly, extend beyond canonical functions of the Smc5/6 complex in chromosome segregation. In addition, our analysis uncovers an unexpected connection between Nse1 and RNA polymerase I (RNAP I) ubiquitination. Specifically, Nse1 promotes the ubiquitination of K408 and K410 in A190, the largest subunit of RNAP I, to induce its degradation. We propose that this mechanism contributes to Smc5/6-dependent rDNA disjunction in response to transcriptional elongation defects.

INTRODUCTION

Post-translational modification of proteins is one of the most frequently used mechanisms to control protein function. These modifications can trigger conformational changes in the substrate, new interactions, or change the subcellular localization and stability of proteins. Ubiquitination is one of the most frequently employed post-translational modifications, consisting in the formation of an isopeptide bond between the C-terminal glycine residue of ubiquitin (Ub) and the ε-amino group of a lysine in the target protein (Komander & Rape, 2012). Ub itself can also be targeted for ubiquitination. To this end, it uses one of its seven lysines as acceptor sites, and giving rise to a wide diversity of ubiquitin chains and possible signaling modes (Komander & Rape, 2012). Depending on the type of Ub chain decoration of the substrate, ubiquitination may be signal for proteasomal degradation, DNA repair, protein trafficking or extraction from a specific compartment or protein complex. Ubiquitination depends on an enzymatic cascade, involving a Ub activating enzyme (E1), a Ub-conjugating enzyme (E2) and a Ub ligase enzyme (E3). In budding yeast, one E1, eleven E2s and a large family of E3 enzymes catalyze the transfer of Ub molecules to specific substrates (Finley *et al*, 2012). Protein ubiquitination is balanced by deubiquitinating proteases, which cleave the isopeptide bond between Ub and the target thus reversing the modification (Piper & Stringer, 2011). Although ubiquitination is regulated at multiple levels, E3 enzymes are strategic players, as they provide specificity to the ubiquitination reaction. Most E3s catalyze the transfer of ubiquitin by bridging the interaction between a Ub-charged E2 enzyme and the substrate. The most abundant type of E3 ligases contain RING domains, which interact with the E2 and reorient the E2-Ub thioester bond to favor the discharge of Ub onto the subatrte (Zheng & Shabek, 2017). Proper folding of RING domains requires the presence of eight conserved cysteine or histidine residues coordinating two zinc atoms in a cross-brace conformation (Borden, 2000). This folding is essential for their E3 activity, and mutation of these residues severely affects ubiquitination of their targets.

Ubiquitination has indispensable roles in DNA repair, by enabling extensive signaling in response to DNA damage and replicative stress (Schwertman *et al*, 2016; Mirsanaye *et al*, 2021). The maintenance of genome integrity also requires the action of the Structural

Maintenance of Chromosome (SMC) complexes, present in all domains of life. SMC complexes use their ATPase activity to form loops and properly organize genomes during chromosome replication, segregation and DNA repair. Particularly, the Smc5/6 complex enables chromosome disjunction by promoting removal of DNA-mediated connections between sister chromatids, which mainly arise during DNA replication and recombinational repair (Torres-Rosell *et al*, 2007; Bermudez-Lopez *et al*, 2010).

The Smc5/6 complex is assembled from eight subunits: Smc5 and Smc6, which constitute the core of the complex, and six non-SMC subunits (Nse proteins), Nse1 to Nse6. Unlike other SMC complexes, Smc5/6 contains two RING domains, located in the C-terminal part of the Nse1 and Nse2 subunits (Solé-Soler & Torres-Rosell, 2020). The RING domain in Nse2 has SUMO ligase activity, while the RING domain in Nse1 has Ub ligase activity (Zhao & Blobel, 2005; Andrews *et al*, 2005; Potts & Yu, 2005; Doyle *et al*, 2010; Hou *et al*, 2012). Nse1 interacts with Nse3, a member of the highly conserved MAGE (melanoma-associated antigen) family of proteins through its N-terminal domain. The central part of Nse1 associates with Nse4, a member of the EID (E1A-like inhibitor of differentiation) family (Hudson *et al*, 2011), to form a subcomplex that then binds to the ATPase domain of Smc5 and the neck region of Smc6. The C-terminal RING domain in Nse1 homologues (NH-RING) is characterized by the presence of a C4HC3 configuration of zinc-coordinating residues, closely related to the PHD (Plant Homology) domain and different from the conventional C3HC4 consensus found in other E3 RING domains (Pebernard *et al*, 2008). Nse1 proteins show other features of Ub E3 ligases, including the capacity to form Ub chains in vitro (Doyle *et al*, 2010; Hou *et al*, 2012). In human cells, Nse1 ubiquitinates Nse3 in vitro, and its E3 ligase activity is enhanced by Nse3 (Doyle *et al*, 2010; Kozakova *et al*, 2015). The human Nse1 targets the cytosolic iron-sulfur assembly (CIA) component Mms19 for its ubiquitination and degradation, with relevant implications in DNA polymerase function and genome stability (Weon *et al*, 2018). However, and differently to Nse2, no other in vivo targets for Nse1 have been identified until now. Although the *NSE1* RING domain is not essential for viability, it promotes DNA repair functions of the Smc5/6 complex (Pebernard *et al*, 2008; Maria *et al*, 2007; Wani *et al*, 2018), and *nse1* mutant cells carrying mutations in zinc-coordinating residues show an aberrant morphology and severe growth defects, particularly under DNA damaging conditions.

To fill the gap in our current knowledge of Nse1-dependent Ub targets, we have analyzed the nuclear ubiquitinome of wild type yeast cells and compared it to *nse1* mutants bearing a C274A mutation in the RING domain (Maria *et al*, 2007). Our analysis indicates that the Nse1 affects the ubiquitination status of several proteins involved in ribosome biogenesis and metabolism. In addition, Nse1 promotes the ubiquitination of two important chromatin-associated factors, Rpa190, the largest subunit in RNA Polymerase I (RNAP I), and Pol30, the proliferating cell nuclear antigen. Moreover, we provide evidence that Nse1 contributes in the Rad6-Rad18-Pol30 pathway for repair of alkylation damage and show that it endorses ubiquitination of RNAP I complexes to trigger their destruction and facilitate disjunction of the rDNA array. Overall, our study indicates that the RING domain of Nse1 impacts in the ubiquitination of several targets that extend beyond canonical functions of the Smc5/6 complex in chromosome segregation.

RESULTS

A proteomic screen to identify Nse1-sensitive ubiquitin sites

To identify Nse1-sensitive ubiquitin sites, we profiled the ubiquitinome of wild type and *nse1-C274A* mutant cells using diGly proteomics (Kim *et al*, 2011). The latter are affected in a conserved zinc-coordinating cysteine residue in the RING domain (Maria *et al*, 2007). As *nse1-C274A* mutant cells are sensitive to DNA damage, and to maximize differences with their wild type counterpart, exponentially growing cultures were treated with 0,02% MMS for 1.5 hours. In addition, we fractionated whole cell extracts into soluble and nuclear fractions to reduce the complexity of the sample. Protein extracts from the nuclear fraction were trypsinized and peptides containing the signature di-glycine remnant from ubiquitin were enriched by immunopurification (Figure 1A). Finally, ubiquitinated peptides from two biological and two technical replicates were quantified by label-free mass-spectrometry (Figure 1A)(Lecona *et al*, 2016). We used the flowthrough from the immunoprecipitation to quantify the total protein content in the nuclear extract, allowing the identification of 3657 proteins. 62 proteins were significantly less expressed (q-value<0.05) and 207 proteins were upregulated in *nse1* samples. Proteins showing higher expression in *nse1* mutant cells were enriched in functions related to purine ribonucleotide metabolism and cellular respiration (FDR 4.32E-2 and 3.90E-2). One of the proteins showing the highest expression in *nse1* mutant cells was Leu2, the auxotrophic marker used for selection of the *nse1-C274A* allele, and an internal control for the total protein quantitation. Proteins less expressed in the *nse1* mutant cells were enriched in functions related to amino acid metabolism (FDRs 2.84E-06 to 3.60E-02). In addition, three proteins encoded by 2μ plasmids (Rep1, Rep2 and Raf1) were down-regulated in the *nse1-C274A* mutant, suggesting that the mutation might restrict the maintenance of episomal plasmids. Interestingly, a recent screen for mutants defective in maintenance of 2μ plasmids identified a variant in the Nse2 subunit of the Smc5/6 complex (Hays *et al*, 2020).

809 of the proteins in the flowthrough (around 20%) were also identified after di-Gly immunoprecipitation (Figure 1B). In total, we found 1932 ubiquitinated sites. The nuclear enrichment step used in our protocol most probably accounts for the lower number of ubiquitinated peptides identified, relative to other studies (Tong *et al*, 2014; Swaney *et al*,

2013). As shown in Figure 1C, 96 diGly-sites were significantly (q-value<0.1) less ubiquitinated in *nse1-C274A* mutant cells, representing potential Smc5/6-dependent targets. Gene ontology analysis revealed that peptides with lower levels of ubiquitylation in *nse1-C274A* cells were enriched in categories related to glycolysis, sterol synthesis, proteasome-mediated destruction, ribosomal proteins and RNA polymerases (Figure 1D). Markov cluster (MCL) analysis of Nse1-dependent high confidence hits revealed the presence of several subclusters, with nodes of ribosomal, glycolysis, RNA polymerase, and sterol biosynthesis proteins (Figure 1E). In addition, we identified one subcluster, containing DNA replication factors, which included Pol30 and ribonucleotide reductase subunits

In accordance with perturbations in ribosomal protein ubiquitination found in our data, *smc5/6* mutants accumulate ribosomal proteins in the nucleus and exhibit ribosome biogenesis defects (Kim *et al*, 2016). In addition, Smc5/6 function has been previously connected to carbon metabolism (Simpson-Lavy *et al*, 2015), and hypomorphic alleles in the human *NSE2* subunit exhibit a metabolic syndrome (Payne *et al*, 2014), phenotypes that could stem from defective ubiquitination of glycolytic enzymes. Overall, the alteration of ubiquitin site usage in *nse1-C274A* mutants indicates that the Nse1 RING domain participates in various cellular processes that, importantly, extend beyond canonical Smc5/6 functions in chromosome replication, segregation and repair.

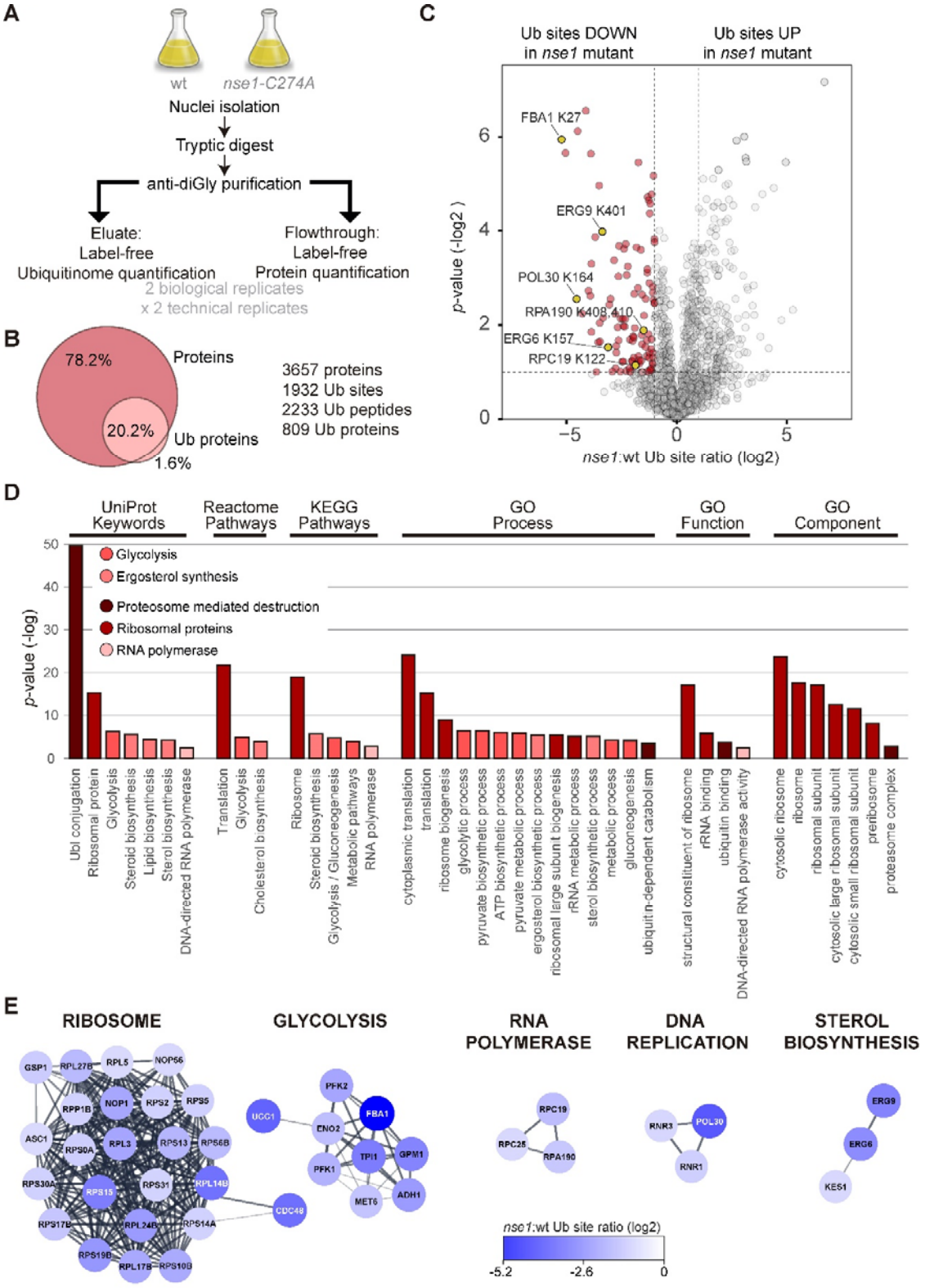
A
wt
nse1-C274A
Nuclei isolation
Tryptic digest
anti-diGly purification
Eluate:
Label-free
Ubiquitinome quantification
Flowthrough:
Label-free
Protein quantification
2 biological replicates
x 2 technical replicates
B
78.2%
Proteins
20.2%
Ub proteins
1.6%
3657 proteins
1932 Ub sites
2233 Ub peptides
809 Ub proteins
C
Ub sites DOWN in nse1 mutant
Ub sites UP in nse1 mutant
FBA1 K27
ERG9 K401
POL30 K164
RPA190 K408,410
ERG6 K157
RPC19 K122
p-value (-log2)
nse1:wt Ub site ratio (log2)
D
UniProt Keywords
Reactome Pathways
KEGG Pathways
GO Process
GO Function
GO Component
Glycolysis
Ergosterol synthesis
Proteosome mediated destruction
Ribosomal proteins
RNA polymerase
p-value (-log)
Ubl conjugation
Ribosomal protein
Glycolysis
Steroid biosynthesis
Lipid biosynthesis
Sterol biosynthesis
DNA-directed RNA polymerase
Translation
Glycolysis
Cholesterol biosynthesis
Ribosome
Steroid biosynthesis
Glycolysis / Gluconeogenesis
Metabolic pathways
RNA polymerase
cytoplasmic translation
translation
ribosome biogenesis
glycolytic process
pyruvate biosynthetic process
ATP biosynthetic process
pyruvate metabolic process
ergosterol biosynthetic process
ribosomal large subunit biogenesis
rRNA metabolic process
sterol biosynthetic process
metabolic process
gluconeogenesis
ubiquitin-dependent catabolism
structural constituent of ribosome
rRNA binding
ubiquitin binding
DNA-directed RNA polymerase activity
cytosolic ribosome
ribosome
ribosomal subunit
cytosolic large ribosomal subunit
cytosolic small ribosomal subunit
preribosome
proteasome complex
E
RIBOSOME
GLYCOLYSIS
RNA POLYMERASE
DNA REPLICATION
STEROL BIOSYNTHESIS
nse1:wt Ub site ratio (log2)
-5.2
-2.6
0

Figure 1. **A proteomic screen to identify Nse1-sensitive ubiquitin sites. A.** Experimental workflow for label-free quantification of ubiquitin sites and total protein levels in nuclear fractions form wild type and *nse1-C274A* mutant cells. 2 biological and two technical replicates were used for each strain. **B**. Venn diagram of proteins identified in nuclear extract (Proteins) and in anti-diGly purification (Ub proteins) and summary of number of proteins, peptides and sites identified. **C.** Volcano plot showing the differentially ubiquitinated sites ($\log_2$ ratios) between wild type and *nse1-C274A* mutant cells and their statistical significance ($-\log_{10}$(*p*-value)) on the y-axis; significantly affected sites are shown above the dotted line; the ubiquitin sites down-regulated in *nse1-C274A* cells are shown in red on the left side; the position of specific ubiquitination sites is shown in yellow in the graph. **D.** Gene ontology analysis of ubiquitinated sites downregulated in *nse1-C274A* cells. **E.** Cytoscape Markov cluster analysis of ubiquitin sites significantly down-regulated in *nse1-C274A* cells. Note the presence of a cluster of (mainly) ribosomal proteins, proteins involved in glycolytic functions, RNA polymerase subunits, DNA replication factors and ergosterol biosynthesis enzymes.

Mutation of the RING domain in *NSE1* disrupts Pol30 ubiquitination

According to our proteomic data, K164 in Pol30 is highly affected in *nse1-C274A* cells (Figure 1C). Pol30 is the sliding clamp or proliferating cell nuclear antigen (PCNA) and its ubiquitination at K164 invokes different DNA damage tolerance (DDT) mechanisms in response to DNA lesions during replication. Monoubiquitination depends on Rad6-Rad18 E2-E3 enzymes, and promotes an error-prone DNA lesion bypass; subsequent polyubiquitination by the Mms2-Ubc13 heterodimeric E2 and the Rad5 E3 ligase activates an error-free lesion bypass (Ulrich, 2009).

To validate Pol30 ubiquitination levels in *nse1-C274A* mutant cells we tested its modification status in ubiquitin pull downs from cultures treated with MMS 0,02% for 1,5 hours. Protein extracts were prepared under denaturing conditions and 7xHis-tagged ubiquitin, expressed from the *CUP1* promoter, was pulled down with NiNTA beads. As a control for ubiquitinated Pol30 species, we used cells that carry a K164R mutation on *POL30*, which abolishes Pol30 ubiquitination. As shown in Figure 2A, MMS treatment triggered similar DNA damage checkpoint responses in both wild type and *nse1-C274A cells*, as determined by western blot analysis of Rad53 phosphorylation. Pull down analysis of ubiquitinated species confirmed that MMS induced the ubiquitination of Pol30 in wild type cells, and that this modification is dependent on K164 of Pol30, as previsouly described. However, the level of ubiquitinated Pol30 species was substantially lower in

nse1-C274A cells, indicating that *NSE1* plays an important role in mono- and polyubiquitination of Pol30.

To further corroborate these findings, we used a different *nse1* mutant, carrying mutations in two other conserved zinc-coordinating residues (H306A and C309A; hereafter referred to as *nse1-AA* mutant) (Wani *et al*, 2018). Haploid *nse1-AA* mutant cells were constructed by integration of the mutated sequence at the endogenous locus of a wild type diploid strain, followed by sporulation and tetrad dissection. Addition of a C-terminal m7H tag substantially improved growth of the *nse1-AA* cells, relative to *nse1-AA* cells bearing a bulkier or no tag at all (Figure 2B). To avoid possible alterations caused by expression of tagged ubiquitin or Pol30, we directly monitored Pol30 ubiquitylation in protein extracts. As Pol30 can also be SUMOylated by Siz1, we used different controls to identify the different Pol30 species, including extracts from *mms2*Δ (to avoid Pol30 poly-ubiquitination), *siz1*Δ (to avoid Pol30 SUMOylation at K164), 6His-Flag-SUMO (to increase the molecular weight of SUMOylated Pol30), and *K164R* mutant cells. As shown in Figure 2C ubiquitination of Pol30 can be detected as MMS-inducible K164-dependent bands. Importantly, Pol30 mono- and poly-ubiquitination levels were very low in *nse1-AA* cells (Figure 2C). Of note, expression of a wild type *NSE1* gene fused to the m7H tag sensitized cells to MMS and also downregulated Pol30 polyubiquitylation (Figures 2C and D). Altogether, these results confirm a role for Nse1 in Pol30 ubiquitination in response to DNA damage.

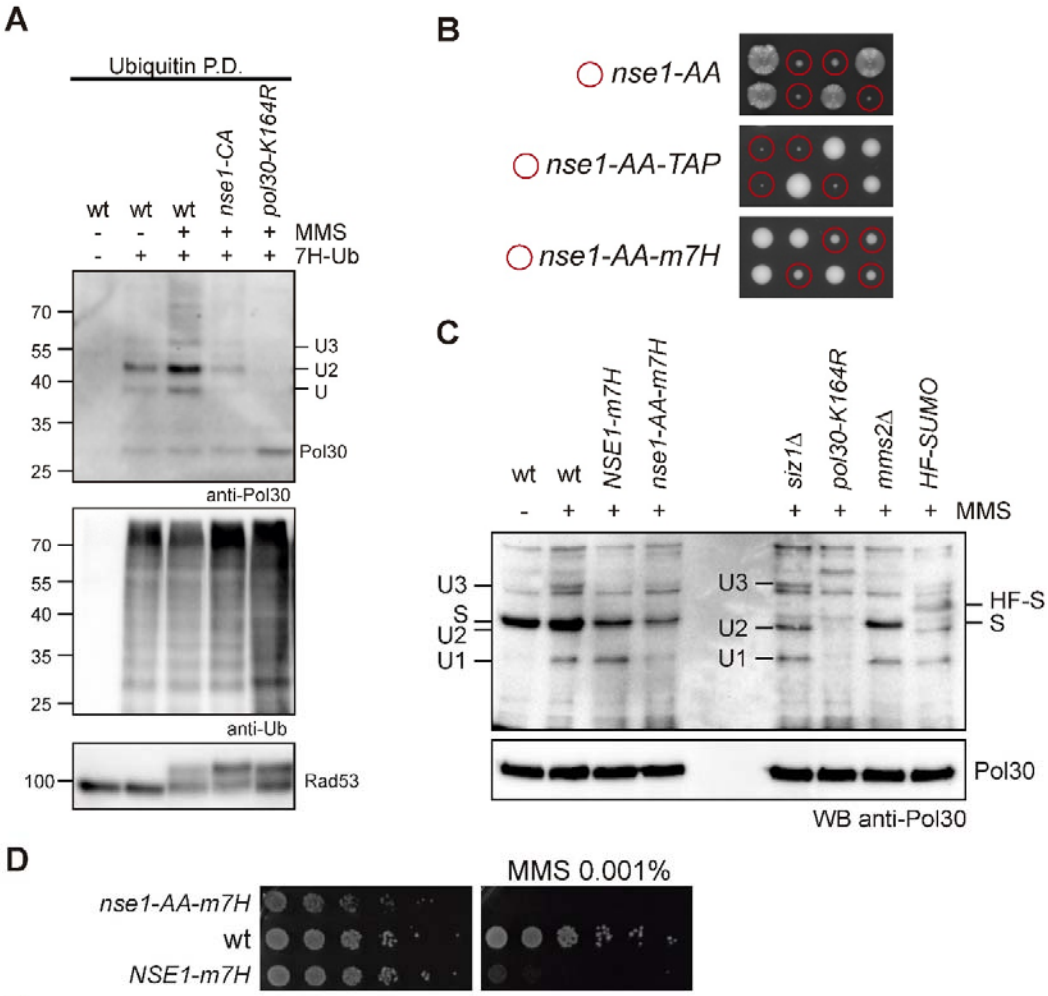
A
Ubiquitin P.D.
wt wt wt nse1-CA pol30-K164R
MMS
7H-Ub
70
55
40
35
25
U3
U2
U
Pol30
anti-Pol30
anti-Ub
100
Rad53
B
nse1-AA
nse1-AA-TAP
nse1-AA-m7H
C
wt wt NSE1-m7H nse1-AA-m7H siz1Δ pol30-K164R mms2Δ HF-SUMO
MMS
U3
S
U2
U1
HF-S
Pol30
WB anti-Pol30
D
MMS 0.001%
nse1-AA-m7H
wt
NSE1-m7H
E
MMS
0.00006%
0.00012%
0.00024%
wt
nse1-CA
rad6Δ
rad6Δ nse1-CA
rad18Δ
rad18Δ nse1-CA
UV
100 μJ/cm2
200 μJ/cm2
400 μJ/cm2

Figure 2. Mutation of the RING domain in *NSE1* disrupts Pol30 ubiquitination. A. Pull down analysis of Pol30 ubiquitination in wild type (wt) and *nse1-C274A* mutant cells, expressing (+) or not (-) 7xHis tagged ubiquitin (7H-Ub) form the *CUP1* promoter; exponentially growing cultures were treated (+) with 0.02% MMS to induce Pol30 ubiquitination; *pol30-K164R* cells were used as control for non-ubiquinated Pol30. **B.** Tetrad dissection analysis of diploid *NSE1/nse1-AA* cells. The mutant nse1 has no tag (top), the TAP tag (medium) or myc-7his (m7H) tag at the C-termins. **C.** Western blot analysis with anti-PCNA (anti-Pol30) antibodies of TCA-protein extracts from the indicated strains. Samples were treated with 0,02% MMS for 1 hour where indicated. S=SUMO-K164; HF-S=6his-Flag-SUMO-K164; U1=PCNA monoubiquitylated at K164; U2=PCNA diubiquitylated at K164; U3=PCNA triubiquitylated at K164; wt= wild type; *mms2Δ* (unable to polyubiquitylate PCNA, lacking U2 and U3 species); *siz1Δ* (unable to SUMOylate PCNA, lacking main SUMOylation band); *K164R=Pol30-K164R* (unable to SUMOylate or ubiquitylate PCNA at K164). **D.** Growth test analysis of wild type of *NSE1* or *nse1-AA* cells tagged with a C-terminal m7H epitope. **E.** Growth test analysis of wild-type, single *nse1-C274A*, *rad6Δ*, *rad18Δ* and double *nse1-C274A rad6Δ, nse1-C274A rad18Δ* cells; 10-fold serial dilutions of the liquid cultures were spotted in YPD in the presence of the indicated MMS concentrations, or irradiated with the indicated doses of UV light, and pictures taken after 48 hours.

Next, we examined if Nse1 acts through the Rad6-Rad18 pathway. To this end, we constructed double *nse1-C274A rad6Δ* and *nse1-C274A rad18Δ* mutants and tested their sensitivity to MMS. As shown in Figure 2E, the *nse1-C274A* mutation slightly impairs the slow growth phenotype *rad6Δ* mutant cells in control plates. However, the *nse1-C274A* mutation did not further sensitize *rad6Δ* or *rad18Δ* cells to MMS, indicating that they are epistatic and operate in the same pathway for alkylation damage repair. In contrast, and as previously described (Maria *et al*, 2007), *nse1-C274A* is additive to *rad6Δ* or *rad18Δ* mutations after UV irradiation, suggesting that Nse1 operates in parallel to Rad6 for repair UV-induced DNA damage. Overall, these results suggest that the RING domain in Nse1 operates in the *RAD6* pathway to promote ubiquitination of Pol30, specifically in response to alkylation damage.

Ubiquitination of lysine 408 and 410 modulates Rpa190 function

Another group of Nse1-dependent ubiquitin targets revealed in our data comprises RNA polymerases. This cluster includes one subunit of RNAP I (Rpa190), a subunit shared by RNAP I and III complexes (Rpc19) and an RNAP III specific subunit (Rpc25). The ubiquitin site showing the greatest difference between wild type and *nse1* mutants is K122 in Rpc19, followed by the double ubiquitination of K408 and K410 in Rpa190. Of note, both Smc5/6

and RNAP I localize and operate in the rDNA array (Torres-Rosell *et al*, 2005; Goodfellow & Zomerdijk, 2013), and inactivation of RNAP I alleviates the rDNA non-disjunction defects of *smc6-9* thermosensitive mutants (Torres-Rosell *et al*, 2007). Therefore, we centered our interest in Rpa190, the largest subunit in RNAP I.

The K408 and K410 residues are located on top of the clamp module in the RNAP I complex, a region that participates in the transition between the open and closed conformation of the polymerase, and close to the Rpa49 subunit, which contributes to elongation (Figure 3A)(Tafur *et al*, 2016; Neyer *et al*, 2016). To study the effect of ubiquitination at K408/K410, we mutated both residues to arginines, generating an *rpa190-K408R,K410R* (hereafter referred to as *rpa190-KR*) allele. This mutant was first expressed from a centromeric plasmid in an *RPA190/rpa190Δ* diploid strain. Tetrad analysis of the progeny showed that *rpa190-KR* mutants are viable and not affected in growth. Next, we integrated the *rpa190-KR* allele and studied the ubiquitination status of the mutant protein using ubiquitin pull downs. As shown in Figure 3B wild type Rpa190 has a prominent ubiquitination band, with an electrophoretic mobility equivalent to a mass increase of around 29 KDa, which might reflect the addition of 3 ubiquitin molecules; besides, there are two extra fainter bands with a mass increase comparable to the addition of 4 and 6 ubiquitin molecules, respectively. As shown in Figure 3B, Rpa190 ubiquitination is severely impaired in *rpa190-KR* cells, with almost no ubiquitination forms detected in the western blot, indicating that ubiquitin mainly targets K408 and K410 in Rpa190.

Rpa190 is deubiquitinated by the Ubp10 ubiquitin peptidase, what prevents its proteasomal degradation (Richardson *et al*, 2012). In accordance, Rpa190 protein levels decreased in *ubp10*Δ cells (Figure 3C). Remarkably, the *rpa190-KR* allele recovered Rpa190 protein levels in *ubp10*Δ mutant cells (Figure 3C). To test if Rpa190 protein and ubiquitination levels are inversely correlated, we performed ubiquitin pull downs in wild type and *ubp10*Δ cells expressing *RPA190* or the *rpa190-KR* alleles from a centromeric plasmid. As previously described (Richardson *et al*, 2012), deletion of *UBP10* led to higher levels of Rpa190 ubiquitination (Figure 3D), an effect that could be also directly detected in protein extracts (Figure 3C). In contrast, ubiquitination was impaired in the Rpa190-KR mutant protein, an effect that was more evident in *ubp10*Δ cells (Figure 3D). Overall, these results

indicate that ubiquitination at lysines K408 and K410 targets Rpa190 for destruction, a process that is normally counteracted by the Ubp10 deubiquitinase.

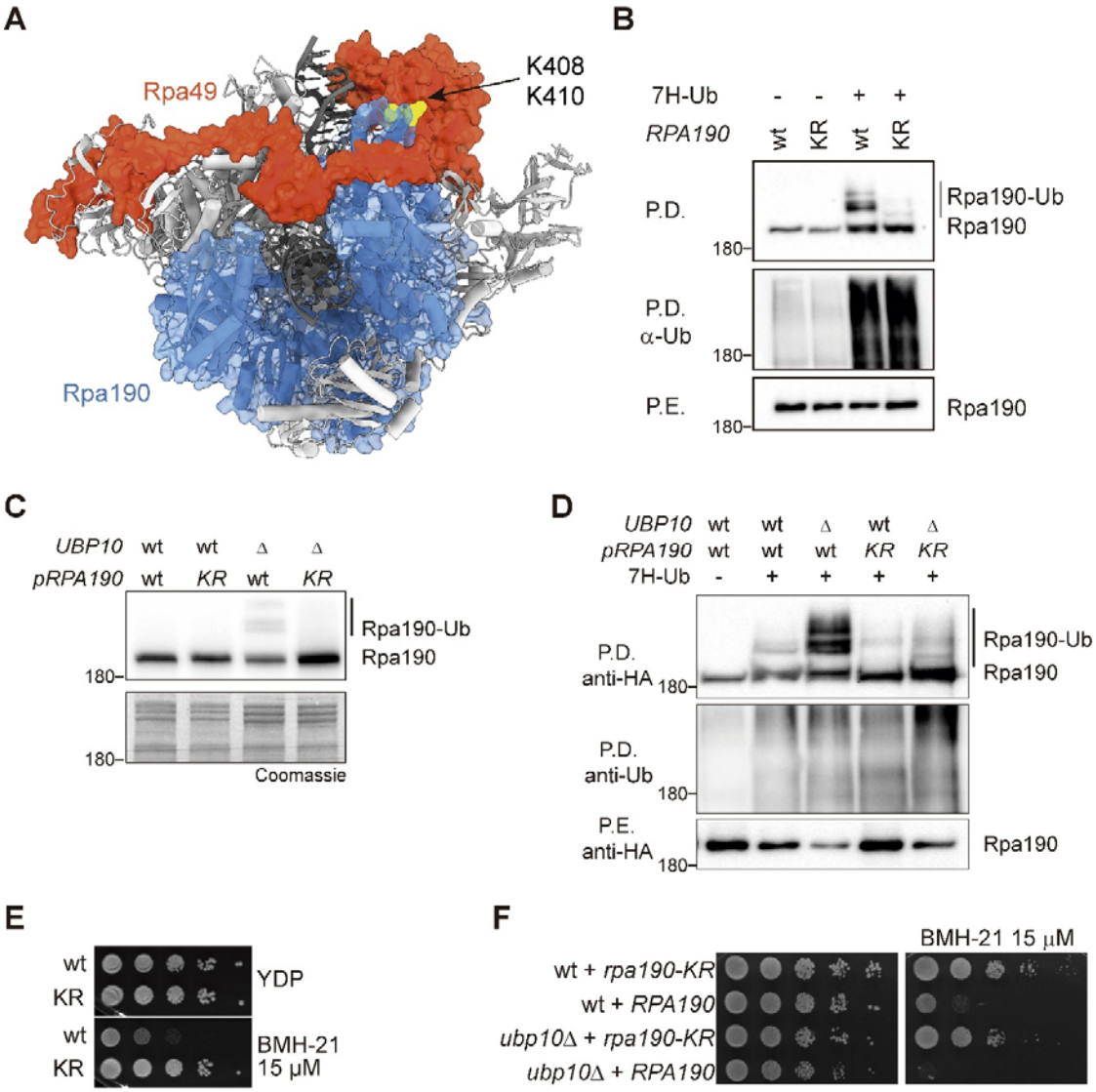

Figure 3. Ubiquitination of lysines 408 and 410 modulates Rpa190 function. A. Structure (PDB 6H68) of an elongating Pol I complex (Sanz-Murillo *et al*, 2018). Rpa190 is shown in blue, Rpa49 in red; K408 and K410 residues in the clamp domain are highlighted in yellow. rDNA and rRNA are shown in dark grey. **B.** Exponentially growing cultures of the indicated strains, expressing (+) or not (-) a 7xHis tagged version of ubiquitin (7H-Ub) from the *CUP1* promoter, were collected; ubiquitinated species from protein extracts (P.E.) were analyzed by pull down (P.D.) of ubiquitinated species under denaturing conditions. 6HA-tagged wild type (wt) or mutant (KR) Rpa190 was detected with anti-HA antibodies. **C.** Western blot analysis of wild type (wt) and *ubp10Δ* (*Δ*) mutant cells, expressing the indicated *RPA190* alleles; wt=wild type, KR=*rpa190-KR*; bottom panel, coomassie staining of the membrane**. D.** Pull down analysis of Rpa190 ubiquitination in wild

type (wt) and *ubp10Δ* (*Δ*) mutant cells expressing the indicated *RPA190* alleles; wt=wild type, KR=rpa190-KR; 7H-Ub=7xHis tagged ubiquitin. **E.** Growth test analysis of wild type (wt) and *rpa190-KR* (KR); 10-fold serial dilutions of the liquid cultures were spotted in in YPD (up) or YPD plus BMH-21 15 μM (bottom). **F.** Wild type (wt) and *ubp10Δ* cells transformed with a centromeric vector expressing the indicated *RPA190* alleles were grown overnight in selective media and spotted in YPD (up) or YPD plus 15 μM BMH-21 (bottom); pictures were taken after 48 hours.

rpa190-KR mutant cells are not sensitive to genotoxic stress or to high temperature. This is in accordance with the observation that Rpa190 ubiquitination does not change in response to DNA damage or with temperature; Rpa190 ubiquitination also did not change at different stages in the cell cycle or in cells with 25 or 190 copies of the rDNA.

Next, we analysed the sensitivity of *rpa190-KR* cells to BMH-21, a specific inhibitor of RNAP I (Peltonen *et al*, 2014). BMH-21 has been proposed to act as a DNA intercalator that inhibits rRNA synthesis by mediating the disassembly of the polymerase from the rDNA and the subsequent degradation of Rpa190 (Peltonen *et al*, 2014; Wei *et al*, 2018). Interestingly, *rpa190-KR* mutant cells are more resistant to BMH-21 (Figure 3E). This suggests that the *rpa190-KR* allele protects cells from BMH-21-mediated Rpa190 degradation. This phenotype is dominant, as expression of an *rpa190-KR* allele from a centromeric vector in wild type cells conferred resistance to BMH-21 (Figure 3F). In addition, *ubp10*Δ mutant cells are more sensitive to BMH-21, as expected from their increased Rpa190 ubiquitination levels. Moreover, ectopic expression of an *rpa190-KR* allele rescued the BMH-21 sensitivity of *ubp10*Δ mutant cells, evidencing that K408 and K410 play a pivotal role in the response to BMH-21. Overall, the phenotype of *rpa190-KR* cells in the presence BMH-21 suggests that Rpa190 ubiquitination at K408 and K410 regulates transcriptional elongation by RNAP I.

An active Smc5/6 complex is required to sustain normal Rpa190 ubiquitination levels

To validate the decrease in Rpa190 ubiquitination in *nse1-RING* mutants, we pulled down 7His-tagged ubiquitin in cells expressing a 6HA-tagged copy of Rpa190. Ubiquitination levels of Rpa190 were lower in *nse1-C274A*, relative to wild type cells (Figure 4A), indicating that this modification is partly dependent on the Nse1 RING domain. The

reduction in Rpa190 ubiquitination in *nse1-C274A* cells is comparable to the one exhibited by *rpa190-KR* cells.

As Pol30 ubiquitination depends on *RAD6*, we analysed if this E2 is also involved in modification of Rpa190. As shown in Figure 4B, Rpa190 ubiquitination levels were lower in *rad6*Δ cells, while they were not affected by the *mms2*Δ mutation. Surprisingly, ubiquitination of Rpa190 was also very low in *cdc34-1* mutants, affected in the E2 catalytic subunit of the Cdc34-SCF ubiquitination complex, indicating that more than one E2 may modify Rpa190.

The Nse2 subunit in the Smc5/6 complex has been reported to promote SUMOylation of Rpa190. Therefore, we speculated that the reduced ubiquitylation of Rpa190-KR might depend on impaired SUMOylation. However, we could not detect differences in Rpa190 SUMOylation between wild type and *rpa190-KR* mutant cells, indicating that the main SUMO target on Rpa190 are not lysines K408 and K410. In addition, our results indicate that Rpa190 ubiquitination is not required for Rpa190 SUMOylation. As both types of Rpa190 modifications seem to depend on the Smc5/6 complex, we reasoned that ubiquitination might require prior SUMOylation. To this end, we analyzed Rpa190 ubiquitination levels in *nse2*Δ*C* mutant cells. Interestingly, Rpa190 ubiquitination was lower in *nse2*Δ*C* mutants, relative to wild type cells (Figure 4C). This suggests that perturbing RNAP I SUMOylation might affect its subsequent ubiquitination. Overall, our results suggest that Smc5/6 function is required to sustain proper Rpa190 ubiquitination levels. Thus, a reduction in Smc5/6 activity might interfere with RNAP I transcriptional elongation, most probably by reducing its ubiquitination at K408 and K410.

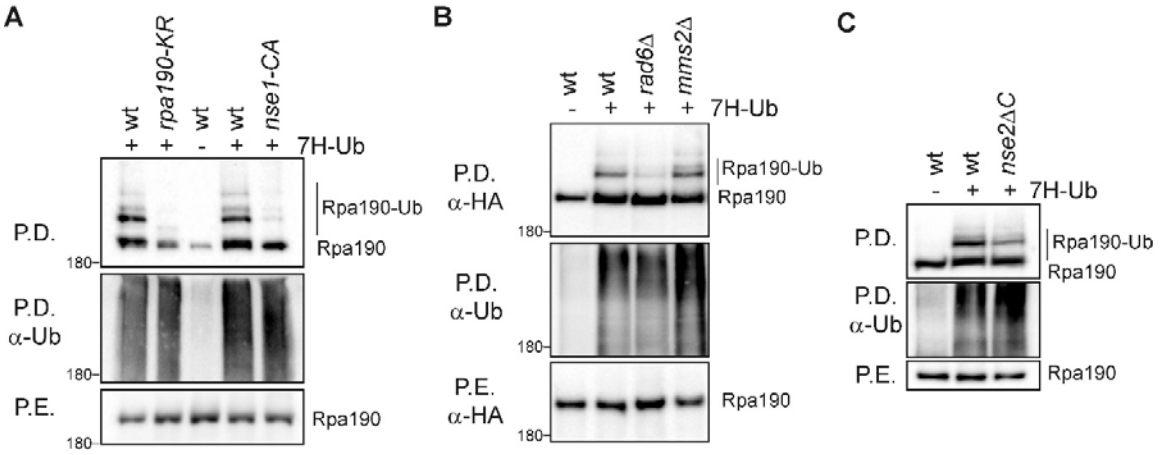

Figure 4. An active Smc5/6 complex is required to sustain normal Rpa190 ubiquitination levels. A. Pull down analysis of Rpa190 ubiquitination in wild type (wt), *rpa190-KR* and *nse1-CA* cells; ubiquitin was pulled down (P.D.) under denaturing conditions from yeast protein extracts (P.E.) to purify ubiquitinated species. **B.** Pull down analysis of Rpa190 ubiquitination in wild type and E2 mutant strains. **C.** Pull down analysis of Rpa190 ubiquitination in wild type and *nse2ΔC* mutant strains.

Rpa190 ubiquitination improves rDNA segregation in *smc5/6* mutants

We have previously shown that RNAP I function is detrimental for rDNA segregation in *smc5/6* mutants (Torres-Rosell *et al*, 2007). Therefore, it is possible that Smc5/6 might promote clearance of transcribing RNAP I through ubiquitination of the Rpa190 subunit in RNAP I, thus ensuring completion of rDNA replication and sister chromatid disjunction. To test this idea, we analysed rDNA segregation, using a battery of tet operators (tetO:487) inserted in the telomeric flank of the rDNA array (Machín *et al*, 2005). Cultures of *smc5/6* mutants cells typically fail to segregate tetO:487 in 50% of the population (Torres-Rosell *et al*, 2005). To inactivate Smc5/6 function, we used an auxin inducible degron allele of *SMC5* (*smc5-aid*). After synchronization of cells in G1 with alpha factor, cultures were treated with auxin to promote Smc5-aid degradation. Next, cells were released from the arrest and observed under the microscope. Cells started budding at 40 minutes, entered anaphase between 80 and 100 minutes, and most of them completed nuclear fission 140 minutes after release from G1 (Figure 5A). Cells with two divided nuclei at time points between 120 and 160 minutes were scored for segregation of tetO:487 operators (Figure 5B). As shown in Figure 5C, the *rpa190-KR* allele significantly aggravates the rDNA segregation defect of *smc5-aid* cells. In contrast, deletion of *UBP10* has the opposite effect and improves rDNA

segregation in *smc5-aid* cells. Therefore, our results indicate that Rpa190 ubiquitination levels affect rDNA segregation in *smc5-aid* mutant cells and suggest that the rDNA segregation defects in *smc5/6* mutant cells partly stem from insufficient Rpa190 ubiquitination. Overall, these observations suggest that Smc5/6-dependent ubiquitination of Rpa190 might be a mechanism to dislodge elongating RNAP I complexes from chromatin, thus preventing non-disjunction events in the rDNA array.

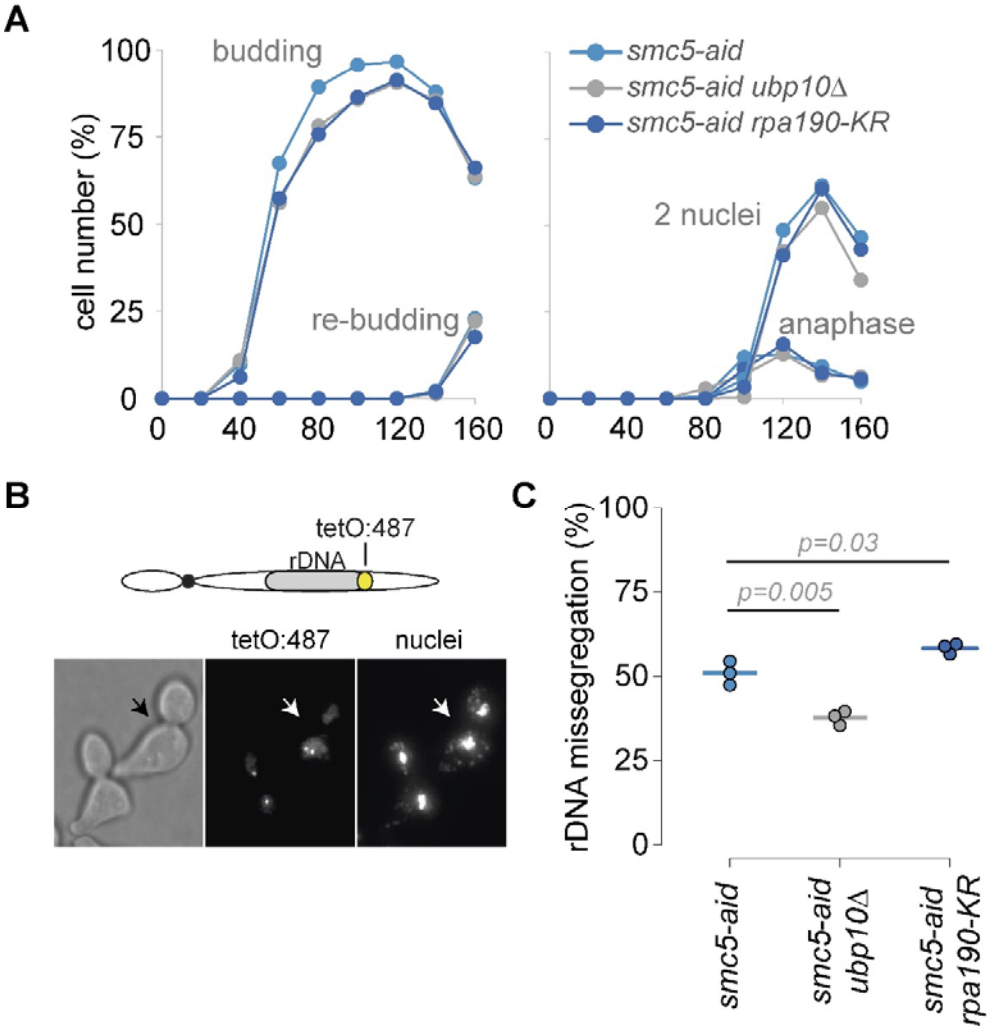

Figure 5. **Rpa190 ubiquitination improves rDNA segregation in *smc5/6* mutants. A.** Cells of the indicated genotype were synchronized in G1 with alpha factor, treated with auxin for 30 min to degrade Smc5-aid and released into a synchronous cell cycle in the presence of auxin. Samples were taken at the indicated time points for microscopic analysis and scored for budding (first S phase), re-budding (second S phase), elongated nucleus between mother and daughter cell (anaphase) and 2 nuclei (two nuclear masses between mother cell and bud). **B.** Around 50% of *smc5-aid* fail to segregate the distal part of the rDNA locus; upper

panel, rDNA segregation was assayed using a battery of fluorescent *tetO* repeats inserted at the indicated position in chromosome XII; bottom panel, representative micrographs of *smc5-aid* cells at time 120 min after G1 release, nuclei stained with Hoetsch; arrow points to cell with missegregated tetO tags. **C.** Quantification of rDNA missegregation in cells of the indicated genotypes. Cells with two nuclei at times 105-160 min after G1 release were scored for rDNA segregation, as shown in B. Circles indicate individual measurements from 3 independent experiments; horizontal lines show medians; *p*=*p*-value, ANOVA test.

DISCUSSION

A proteomic approach to identify Nse1-dependent ubiquitin targets

The notion that inactivation of the RING domain in Nse1 impairs cell growth and sensitizes cells to DNA damage highlights its important functions in cell proliferation and genome integrity (Maria *et al*, 2007; Pebernard *et al*, 2008; Wani *et al*, 2018). In humans, Nse1 has ubiquitin E3 ligase activity *in vitro*. This activity is enhanced by the interaction with MAGE proteins, the mammalian orthologs of the Nse3 subunit (Doyle *et al*, 2010). However, the only *in vivo* substrate identified for Nse1 is Mms19, a cytosolic iron-sulfur assembly (CIA) component (Weon *et al*, 2018). Our label-free proteomic approach has allowed us to identify a large set of Nse1-dependent ubiquitin targets, and to reveal novel and important connections of Nse1 with DNA replication and DNA damage tolerance, ribosomal biogenesis and cell metabolism. Thus, our study should constitute a valuable source of information about the ubiquitin-dependent processes and pathways affected by the RING domain in Nse1.

Network analysis of Nse1-dependent ubiquitin targets exposes several functional clusters (Figure 1). Interestingly, a large set of proteins, including Pol I subunits, RNA processing elements and ribosomal proteins, show deregulated ubiquitination in *nse1* mutants cells, which points to ribosome biogenesis as one of the main processes controlled by Nse1. This is in accordance with the previously reported nuclear accumulation of ribosome subunits exhibited by both *smc5/6* and *nse2Δ*RING* mutants (Kim *et al*, 2016), which could result from deficient controls during ribosome biogenesis. Given the relevance of ribosome biogenesis for optimal cell growth and proliferation, it is possible that the impaired fitness of *nse1* mutant cells (Maria *et al*, 2007; Wani *et al*, 2018) may be partly due to defects in ribosome synthesis.

Another group of ubiquitin targets identified in our study is related to glycolytic processes that, apparently, are not directly related to Smc5/6 or Nse1 functions on chromatin. Nevertheless, it is worth noting that previous studies have also established a connection between the Smc5/6 complex and carbon metabolism (Simpson-Lavy *et al*, 2015). Moreover, hypomorphic *NSMCE2* mutations identified in two patients have been related to a human syndrome linked to dwarfism, insulin resistance and severe metabolic

abnormalities (Payne *et al*, 2014). Altogether, these data suggest a role for the Smc5/6 complex in the regulation of metabolic processes through the control of protein ubiquitination.

Regulation of PCNA ubiquitination by Nse1

One of the most prominent ubiquitin targets identified in our proteomic screen is K164 in Pol30 (PCNA). PCNA is known to be monoubiquitinated at K164 by Rad6-Rad18 and further polyubiquitinated with K63-linked ubiquitin chains by Mms2-Ubc13-Rad5 (Hoege *et al*, 2002; Parker & Ulrich, 2009). PCNA mono-ubiquitination enables DNA replication at damaged forks by recruiting translesion synthesis polymerases, while PCNA polyubiquitination promotes template switch behind the fork, to enable the bypass of lesions on the template (Ulrich, 2009). Notably, a direct link between the Smc5/6 complex and the enzymes responsible for PCNA ubiquitination has been previously demonstrated in vertebrates: Rad18 interacts with the Nse5-Nse6 homologs to recruit the Smc5/6 complex to interstrand crosslinks, a burdensome lesion that stalls replication forks (Räschle *et al*, 2015). Our results suggest that Nse1 may act in concert with Rad18 and Rad6 to ubiquitinate PCNA (Figure 2). PCNA ubiquitination in vitro is very inefficient and requires prior RFC-dependent loading of PCNA onto partially heteroduplex DNA (Garg & Burgers, 2005; Haracska *et al*, 2006). It is worth noting that PCNA ubiquitination in vivo occurs in a context of damaged and partially replicated chromatin fibers behind a fork, a situation that could require the participation of Nse1 and the Smc5/6 complex. In accordance, the Smc5/6 complex is also recruited to damaged forks (Lindroos *et al*, 2006; Bustard *et al*, 2012). The participation of Nse1 in PCNA ubiquitination is further supported by the epistasic relation between *NSE1* and *RAD6-RAD18* during alkylation damage. The observation that Nse1 and Rad6-Rad18 are not epistatic for UV-born lesions (Maria *et al*, 2007) suggests that different types of lesions may have different requirements for activation of DNA damage tolerance. We thus propose that, in response to alkylation damage, Nse1 is an additional player required for PCNA ubiquitination, probably through direct interactions with Rad18 and/or Rad6. We cannot discard the possibility that Nse1 plays an ancillary role in Pol30 ubiquitination, perhaps by reconfiguring the topology of damaged replication forks, in an unknown way, to prime full PCNA ubiquitination. Further

experiments will be required to elucidate the mechanisms used by Nse1 in PCNA ubiquitination.

A role for Nse1-dependent ubiquitination in Pol I transcriptional elongation

Another ubiquitin target identified in our screen is Rpa190, the large subunit of Pol I. Based on our proteomics and pull-down experiments, we propose that ubiquitination of lysines 408 and 410 depends on Nse1. Of note, Smc5/6 and RNAP I show some interesting connections. First, both of them bind to the rDNA array (Torres-Rosell *et al*, 2005) (Russell & Zomerdijk, 2006); besides, RNAP I is SUMOylated in an Nse2-dependent manner (Albuquerque *et al*, 2013); in addition, inactivation of RNAP I partially relieves the rDNA missegregation phenotype of *smc5/6* mutants (Torres-Rosell *et al*, 2007).

DNA damage or cell cycle arrests do not alter Rpa190 ubiquitination. In contrast, amino acid starvation dramatically decreases Rpa190 ubiquitination. Limited nutrient availability causes a reduction in rRNA synthesis through proteasomal degradation of Rrn3, which is required for Pol I recruitment to the rDNA promoter (Philippi *et al*, 2010). Thus, Rpa190 ubiquitination is reduced when Pol I transcription initiation ceases. In accordance, Rpa190 ubiquitination requires actively transcribing Pol I complexes on chromatin (Bunney *et al*, 2017). Nse1-dependent Rpa190 ubiquitination may trigger its degradation by the proteasome, a situation that is normally counteracted by the Ubp10 ubiquitin protease (Richardson *et al*, 2012; Bunney *et al*, 2017). The analysis of double *rpa190-KR* and *ubp10*Δ mutants indicates that K408 and K410 are the relevant targets for ubiquitin-dependent Rpa190 degradation. We speculate that cells may ubiquitinate arrested Pol I complexes to degrade them and prevent further interferences with other transactions at the rDNA locus, including collisions between RANP I and replication forks. As ongoing RNAP I run into DNA replication and repair processes, Nse1 dependent-ubiquitination may promote RNAP I clearance from chromatin and allow resolution of sister rDNAs. In accordance, we have shown that preventing Rpa190 deubiquitination (in *ubp10Δ* cells) improves rDNA missegregation in Smc5/6 mutant cells, while the *rpa190-KR* mutant worsens it. Thus, Rpa190 ubiquitination should enable disjunction of the rDNA array, helping to maintain its integrity. In addition, the localization of the ubiquitination sites in Rpa190, at the tip of the clamp domain (Figure 3A), might shed new clues about the role

of this modification. During initiation of transcription, the cleft aperture in RNAP I changes from an open conformation when bound to the Rrn3 transcription factor, to a fully closed configuration in the elongating complex (Fernández-Tornero, 2018; Engel *et al*, 2018). In addition, the Rpa49 linker crosses on top of the cleft, passes over the downstream rDNA, and binds just behind the clamp domain, acting as a safety belt and securing the rDNA inside the transcribing RNAP I complex. Ubiquitination sites in Rpa190 lay close to the path followed by the Rpa49 linker domain, whose roles seem to be the stable clamping of the rDNA during transcriptional elongation. Thus, we hypothesize that ubiquitination at the tip of the clamp might interfere with Rpa49, perhaps reducing the processivity of RNAP I in preparation for its unloading from the rDNA.

One intriguing aspect of our study is that *rpa190-KR* mutants are globally healthy and do not exhibit other phenotypes in common with Smc5/6 mutants, such as sensitivity to DNA damage. However, it is worth noting that we identified other ubiquitin sites in RNAP I being significantly less ubiquitinated in *nse1-C274A* mutant cells. For example, Rpc19, a subunit shared by RNAP I and RNAP III, showed lower ubiquitination on two different sites (with 3.5 and 2.6 fold reduction) in *nse1* mutant, relative to wild type. In comparison, Rpa190 ubiquitination at both K408 and K410 was reduced 2.8 fold in *nse1* mutant extracts. In addition, K120 in Rpa34 and K88 in Rpa43 were also less ubiquitinated in *nse1* mutants, although to a lower extent (1.4 and 1.7 fold reduction relative to the wild type, respectively). Moreover, our proteomic screen allowed us to identify five additional sites under-ubiquitinated in *nse1* mutant cells (two sites in Rpa190 and one in Rpa135, Rpb5 and Rpb10), although differences were not statistically significant, relative to the wild type. Therefore, we currently cannot exclude that other ubiquitinated lysines also participate in RNAP I regulation. In summary, if ubiquitin redundantly targets multiple sites in RNAP I, the modification of other lysines in the complex may be masking a more severe phenotype in *rpa190-K408,410R* cells. Thus, it will be interesting to extend RNAP I KR mutations to other Nse1-dependent sites. We predict that this mutant will evidence a more direct connection to Smc5/6-dependent functions.

Interestingly, *rpa190-KR* mutants are resistant to BMH-21, a specific inhibitor of RNAP I. The resistance of *rpa190-KR* cells to BMH-21, which has been proposed as a tool to treat

cancer cells, opens the question about what is the nature of the problem generated by this inhibitor. BMH-21 is believed to bind G-C rich areas at the rDNA and to block transcriptional elongation by RNAP I (Peltonen *et al*, 2014; Wei *et al*, 2018). However, the resistance of non-ubiquitinable *rpa190-KR* mutants suggests that the sensitivity of wild type cells to BMH-21 is primarily due to Rpa190 ubiquitination and destruction, and not to the inability to proceed with transcriptional elongation. As yeast and human cells are equipped with tools to ubiquitinate and degrade Rpa190, analysis of the physiological situations and mechanisms that trigger RNAP I ubiquitination in cancer cells will be of great interest.

REFERENCES

Albuquerque CP, Wang G, Lee NS, Kolodner RD, Putnam CD & Zhou H (2013) Distinct SUMO ligases cooperate with Esc2 and Slx5 to suppress duplication-mediated genome rearrangements. *PLoS Genet.* **9:** e1003670

Andrews EA, Palecek J, Sergeant J, Taylor E, Lehmann AR, Watts FZ, Fousteri M, Sweeney S & Shinagawa H (2005) Nse2, a component of the Smc5-6 complex, is a SUMO ligase required for the response to DNA damage. *Mol. Cell. Biol.* **25:** 185–196

Bermudez-Lopez M, Ceschia A, de Piccoli G, Colomina N, Pasero P, Aragon L & Torres-Rosell J (2010) The Smc5/6 complex is required for dissolution of DNA-mediated sister chromatid linkages . *Nucleic Acids Res.* **38:** 6502–6512

Borden KLB (2000) Ring domains: Master builders of molecular scaffolds? *J. Mol. Biol.* **297:** 1027

Bunney PE, Zink AN, Holm AA, Billington CJ & Kotz CM (2017) Orexin activation counteracts decreases in nonexercise activity thermogenesis (NEAT) caused by high-fat diet. *Physiol. Behav.* **176:** 139–148

Bustard DE, Menolfi D, Jeppsson K, Ball LG, Carter S, Shirahige K, Sjögren C, Branzei D, Cobb JA, Dewey SC & Sjogren C (2012) During replication stress, non-SMC element 5 (NSE5) is required for Smc5/6 protein complex functionality at stalled forks . *J. Biol. Chem.* **287:** 11374–11383

Doyle JM, Gao J, Wang J, Yang M & Potts PR (2010) MAGE-RING protein complexes comprise a family of E3 ubiquitin ligases . *Mol. Cell* **39:** 963–974

Engel C, Neyer S & Cramer P (2018) Distinct Mechanisms of Transcription Initiation by RNA Polymerases i and II. *Annu. Rev. Biophys.* **47:** 425–446

Fernández-Tornero C (2018) RNA polymerase I activation and hibernation: unique mechanisms for unique genes. *Transcription* **9:** 248–254

Finley D, Ulrich HD, Sommer T & Kaiser P (2012) The ubiquitin-proteasome system of Saccharomyces cerevisiae. *Genetics* **192:** 319–360

Garg P & Burgers PM (2005) Ubiquitinated proliferating cell nuclear antigen activates translesion DNA polymerases eta and REV1. *Proc. Natl. Acad. Sci. U. S. A.* **102:** 18361–6

Goodfellow SJ & Zomerdijk JCBM (2013) Basic mechanisms in RNA polymerase I transcription of the ribosomal RNA genes. *Subcell. Biochem.* **61:** 211–236

Haracska L, Unk I, Prakash L & Prakash S (2006) Ubiquitylation of yeast proliferating cell nuclear antigen and its implications for translesion DNA synthesis. *Proc. Natl. Acad. Sci. U. S. A.* **103:** 6477–82

Hays M, Young JM, Levan PF & Malik HS (2020) A natural variant of the essential host gene MMS21 restricts the parasitic 2-micron plasmid in Saccharomyces cerevisiae. *Elife* **9:** 1–40

Hoege C, Pfander B, Moldovan GL, Pyrowolakis G & Jentsch S (2002) RAD6-dependent DNA repair is linked to modification of PCNA by ubiquitin and SUMO. *Nature* **419:** 135–141

Hou X, Zhang W, Xiao Z, Gan H, Lin X, Liao S & Han C (2012) Mining and characterization of ubiquitin E3 ligases expressed in the mouse testis. *BMC Genomics* **13:** 495

Hudson JJR, Bednarova K, Kozakova L, Liao C, Guerineau M, Vidot S, Marek J, Bathula SR, Lehmann AR, Palecek J, Colnaghi R, Vidot S, Marek J, Bathula SR, Lehmann AR & Palecek J (2011) Interactions between the Nse3 and Nse4 components of the SMC5-6 complex identify evolutionarily conserved interactions between MAGE and EID Families . *PLoS One* **6:** e17270

Janke C, Magiera MM, Rathfelder N, Taxis C, Reber S, Maekawa H, Moreno-Borchart A, Doenges G, Schwob E, Schiebel E & Knop M (2004) A versatile toolbox for PCR-based tagging of yeast genes: new fluorescent proteins, more markers and promoter substitution cassettes . *Yeast* **21:** 947–962

Kim DH, Harris B, Wang F, Seidel C, McCroskey S & Gerton JL (2016) Mms21 SUMO ligase activity promotes nucleolar function in Saccharomyces cerevisiae. *Genetics* **204:** 645–658

Kim W, Bennett EJ, Huttlin EL, Guo A, Li J, Possemato A, Sowa ME, Rad R, Rush J, Comb MJ, Harper JW & Gygi SP (2011) Systematic and quantitative assessment of the ubiquitin-modified proteome. *Mol. Cell* **44:** 325–40

Komander D & Rape M (2012) The Ubiquitin Code. *Annu. Rev. Biochem.* **81:** 203–229

Kozakova L, Vondrova L, Stejskal K, Charalabous P, Kolesar P, Lehmann AR, Uldrijan S, Sanderson CM, Zdrahal Z & Palecek JJ (2015) The melanoma-associated antigen 1 (MAGEA1) protein stimulates the E3 ubiquitin-ligase activity of TRIM31 within a TRIM31-MAGEA1-NSE4 complex. *Cell Cycle* **14:** 920–930

Lecona E, Rodriguez-Acebes S, Specks J, Lopez-Contreras AJ, Ruppen I, Murga M, Muñoz J, Mendez J & Fernandez-Capetillo O (2016) USP7 is a SUMO deubiquitinase essential for DNA replication. *Nat. Struct. Mol. Biol.* **23:** 270–277

Lindroos HB, Ström L, Itoh T, Katou Y, Shirahige K, Strom L, Itoh T, Katou Y, Shirahige K, Sjogren C, Stro L, Sjo C & Ström L (2006) Chromosomal association of the Smc5/6 complex reveals that it functions in differently regulated pathways. *Mol. Cell* **22:** 755–767

Machín F, Torres-Rosell J, Jarmuz A, Aragón L, Machin F, Torres-Rosell J, Jarmuz A & Aragon L (2005) Spindle-independent condensation-mediated segregation of yeast ribosomal DNA in late anaphase. *J. Cell Biol.* **168:** 209–219

Maria SRS, Gangavarapu V, Johnson RE, Prakash L & Prakash S (2007) Requirement of Nse1, a subunit of the Smc5-Smc6 complex, for Rad52-dependent postreplication repair of UV-Damaged DNA in Saccharomyces cerevisiae. *Mol. Cell. Biol.* **27:** 8409–8418

Mirsanaye AS, Typas D & Mailand N (2021) Ubiquitylation at Stressed Replication Forks: Mechanisms and Functions. *Trends Cell Biol.* **31:** 584–597

Neyer S, Kunz M, Geiss C, Hantsche M, Hodirnau V-V, Seybert A, Engel C, Scheffer MP, Cramer P & Frangakis AS (2016) Structure of RNA polymerase I transcribing ribosomal DNA genes. *Nature* **540:** 607–610

Parker JL & Ulrich HD (2009) Mechanistic analysis of PCNA poly-ubiquitylation by the ubiquitin protein ligases Rad18 and Rad5. *EMBO J.* **28:** 3657–66

Payne F, Colnaghi R, Rocha N, Seth A, Harris J, Carpenter G, Bottomley WE, Wheeler E, Wong S, Saudek V, Savage D, O'Rahilly S, Carel JC, Barroso I, O'Driscoll M & Semple R (2014) Hypomorphism in human NSMCE2 linked to primordial dwarfism and insulin resistance. *J. Clin. Invest.* **124:** 4028–4038

Pebernard S, Perry JJP, Tainer JA, Boddy MN, Vidyapeetham AV & Kollam CPO (2008) Nse1 RING-like domain supports functions of the Smc5-Smc6 holocomplex in genome stability. *Mol. Biol. Cell* **19:** 4099–4109

Peltonen K, Colis L, Liu H, Trivedi R, Moubarek MS, Moore HM, Bai B, Rudek MA, Bieberich CJ & Laiho M (2014) A targeting modality for destruction of RNA polymerase I that possesses anticancer activity. *Cancer Cell* **25:** 77–90

Philippi A, Steinbauer R, Reiter A, Fath S, Leger-Silvestre I, Milkereit P, Griesenbeck J & Tschochner H (2010) TOR-dependent reduction in the expression level of Rrn3p lowers the activity of the yeast RNA Pol I machinery, but does not account for the strong inhibition of rRNA production. *Nucleic Acids Res.* **38:** 5315–5326

Piper RC & Stringer DK (2011) Terminating protein ubiquitination: Hasta la vista, ubiquitin. *Cell Cycle* **10:** 3067–3071

Potts PR & Yu HT (2005) Human MMS21/NSE2 is a SUMO ligase required for DNA repair. *Mol. Cell. Biol.* **25:** 7021–7032

Räschle M, Smeenk G, Hansen RK, Temu T, Oka Y, Hein MY, Nagaraj N, Long DT, Walter JC, Hofmann K, Storchova Z, Cox J, Bekker-Jensen S, Mailand N & Mann M (2015) Proteomics reveals dynamic assembly of Repair complexes during bypass of DNA cross-links. *Science (80-.).* **348:** 1253671

Richardson LA, Reed BJ, Charette JM, Freed EF, Fredrickson EK, Locke MN, Baserga SJ & Gardner RG (2012) A Conserved Deubiquitinating Enzyme Controls Cell Growth by Regulating RNA Polymerase I Stability. *Cell Rep.* **2:** 372–385

Russell J & Zomerdijk JCBM (2006) The RNA polymerase I transcription machinery. *Biochem. Soc. Symp.* **73:** 203–216

Sanz-Murillo M, Xu J, Belogurov GA, Calvo O, Gil-Carton D, Moreno-Morcillo M, Wang D & Fernández-Tornero C (2018) Structural basis of RNA polymerase I stalling at UV light-induced DNA damage. *Proc. Natl. Acad. Sci. U. S. A.* **115:** 8972–8977

Schwertman P, Bekker-Jensen S & Mailand N (2016) Regulation of DNA double-strand break repair by ubiquitin and ubiquitin-like modifiers. *Nat. Rev. Mol. Cell Biol.* **17:** 379–394

Simpson-Lavy KJ, Bronstein A, Kupiec M & Johnston M (2015) Cross-Talk between Carbon Metabolism and the DNA Damage Response in S. cerevisiae. *Cell Rep.* **12:** 1865–

1875

Solé-Soler R & Torres-Rosell J (2020) Smc5/6, an atypical SMC complex with two RING-type subunits. *Biochem. Soc. Trans.* **48:** 2159–2171

Swaney DL, Beltrao P, Starita L, Guo A, Rush J, Fields S, Krogan NJ & Villén and J (2013) Global analysis of phosphorylation and ubiquitylation crosstalk in protein degradation. *Nat. Methods* **10:** 1–20

Tafur L, Sadian Y, Hoffmann NA, Jakobi AJ, Wetzel R, Hagen WJH, Sachse C & Müller CW (2016) Molecular Structures of Transcribing RNA Polymerase I. *Mol. Cell* **64:** 1135–1143

Tong Z, Kim MS, Pandey A & Espenshade PJ (2014) Identification of candidate substrates for the golgi tul1 E3 ligase using quantitative diGly proteomics in yeast. *Mol. Cell. Proteomics* **13:** 2871–2882

Torres-Rosell J, Mahín F, Farmer S, Jarmuz A, Eydmann T, Dalgaard JZ & Aragón L (2005) SMC5 and SMC6 genes are required for the segregation of repetitive chromosome regions. *Nat. Cell Biol.* **7:** 412–419

Torres-Rosell J, De Piccoli G, Cordon-Preciado V, Farmer S, Jarmuz A, Machin F, Pasero P, Lisby M, Haber JE & Aragón L (2007) Anaphase onset before complete DNA replication with intact checkpoint responses. *Science (80-.).* **315:** 1411–1415

Ulrich HD (2009) Regulating post-translational modifications of the eukaryotic replication clamp PCNA. *DNA Repair (Amst).* **8:** 461–9

Wani S, Maharshi N, Kothiwal D, Mahendrawada L, Kalaivani R & Laloraya S (2018) Interaction of the Saccharomyces cerevisiae RING-domain protein Nse1 with Nse3 and the Smc5/6 complex is required for chromosome replication and stability. *Curr. Genet.* **64:** 599–617

Wei T, Najmi SM, Liu H, Peltonen K, Kucerova A, Schneider DA & Laiho M (2018) Small-Molecule Targeting of RNA Polymerase I Activates a Conserved Transcription Elongation Checkpoint. *Cell Rep.* **23:** 404–414

Weon JL, Yang SW & Potts PR (2018) Cytosolic Iron-Sulfur Assembly Is Evolutionarily Tuned by a Cancer-Amplified Ubiquitin Ligase. *Mol. Cell* **69:** 113-125.e6

Zhao XL & Blobel G (2005) A SUMO ligase is part of a nuclear multiprotein complex that affects DNA repair and chromosomal organization. *Proc. Natl. Acad. Sci. U. S. A.* **102:** 4777–4782

Zheng N & Shabek N (2017) Ubiquitin Ligases: Structure, Function, and Regulation. *Annu. Rev. Biochem.* **86:** 129–157

METHODS

Ubiquitinome profiling

Protein digestion

To identify Nse1-dependent ubiquitin targets, we isolated the nuclear fraction from 2 l of wild type and *nse1-C274A* mutant yeast cells treated with MMS 0.02% for 1,5 hours, until reaching an OD_{600}~1.5. Cells were harvested for 5 min at 5.000 rpm, resuspended and incubated for 5 min in 400 ml of azide solution (50 mM Tris-Cl-H pH 7.5, azide 0.1% (15 mM)). Next, cells were centrifuged for 5 min at 5.000 rpm, resuspended in 400 ml of reduction solution (500 µl of 1M Tris-HCl pH 7.5, 250 µl β-ME, 49,25 ml H_2O) and incubated 30 min at room temperature. Cells were pelleted and resuspended in 100 ml of SP buffer (1 M sorbitol, 20 mM phosphate buffer pH 7.4) and 2 mg/gr of cells of zymoliase 100T was added to each culture. Then, samples were incubated at 25ºC for 20-25 min at a 100 rpm shaking agitation. After checking spheroplasting, cells were sedimented at 3.200 rpm for 3 min and washed with SP buffer. After removing the supernatant, spheroplasts were resuspended in Ficoll buffer (18% FICOLL, 20 mM phosphate buffer pH 6.8 (PI-Roche, 1 mM EDTA, 5 mM chloroacetamide, 50 µM PR-619)) and kept on ice for 5 min. Samples were centrifuged at 30.000 g for 20 min at 4ºC. Nuclear pellets were lysed in 10 volumes of lysis buffer (5% Sodium deoxycholate, 100 mM Tris, pH 8) supplemented with protease and phosphatase inhibitors (Halt, Pierce). The lysate was incubated at 95ºC 10 minutes and sonicated (20% intensity, 2 min, 1 sec on, 1 sec off). After cooling, 1:1000 (v/v) Benzonase (Merck) was added and further incubated for 1 hour at 37 C. Proteins were reduced and alkylated for 1 h with 15 mM TCEP (Sigma) and 30 mM CAA (Sigma) at RT in the dark. Lysates were diluted 1:5 with 50 mM Tris HCl, pH 8, and proteins were digested with Lys-C (Wako) (enzyme: substrate ratio 1:50) for 6 h. Subsequently, samples were digested overnight at 37 °C with recombinant trypsin (Trypzean, Sigma) (enzyme: substrate ratio 1:50). Enzymes activity were stopped with 2% TFA (v/v). Deoxycholic acid was removed by centrifugal precipitation (20 minutes at 20,000 x g). Peptides present in the supernatant were desalted with 500 mg C18 SepPak SPE cartridges (Waters) and lyophilized.

Immunoprecipitation of di-Gly–containing peptides

Enrichment of K-ε-GG peptides was performed with the PTMScan ubiquitin remnant motif (K-ε-GG) kit (Cell Signaling Technology, cat. no. 5562) containing anti–K-ε-GG antibody cross-linked to protein A beads. Ten milligrams of lyophilized peptides per condition were gently resuspended in 1200 µl of ice cold immunoaffinity purification (IAP) buffer (50 mM MOPS, pH 7.4, 10 mM Na2HPO4, and 50 mM NaCl) and centrifuged at maximal speed for 5 min at 4ºC to remove insoluble materials. The supernatants were mixed with 20 µl of anti–K-ε-GG of pre-conditioned antibody beads and incubated for 2 h at 4°C with rotation. Samples were centrifuged and the supernatant containing the unbound fraction was used to determine the total protein content. Beads were washed twice with 1 ml of ice-cold IAP buffer followed by three washes with ice-cold PBS and two washes with ice-cold MS-grade water. K-ε-GG peptides were eluted from the antibody with 2 × 50 µl of 1% TFA. Eluted peptides were desalted with C18 StageTips conditioned by washing with 80 µl of methanol followed by an equilibration with 80 µl of 1% TFA. Samples were loaded on StageTips, washed twice with 80 µl of 0.1% formic acid FA and eluted with 50 µl 60% MeCN/0.1% (FA). Eluted peptides were dried completely with vacuum centrifugation and reconstituted in 0.1% FA.

Mass spectrometry

LC-MS/MS was carried out by coupling an Ultimate 3000 RSLCnano System (Dionex) with a Q-Exactive HF-X mass spectrometer (ThermoScientific). Samples were loaded into a trap column (Acclaim PepMap^{TM} 100, 100 µm x 2 cm, ThermoScientific) over 3 min at a flow rate of 10 µl/min in 0.1% FA. Then peptides were transferred to an analytical column (PepMap^{TM} RSLC C18, 2 µm, 75 µm x 50 cm, ThermoScientific). The fractions containing di-Gly-containing peptides were separated using a 60 min effective linear gradient (buffer A: 0.1% FA; buffer B: 100% ACN, 0.1% FA) at a flow rate of 250 nL/min. The gradient used was: 0-3 min 2% B, 3-5 min 6% B, 5-36 min 17.5% B, 36-60 min 25% B, 60-63 min 33% B, 63-65 min 45% B, 65-70 min 98% B, 70-80 min 2% B. The peptides were electrosprayed (1.9 kV) into the mass spectrometer through a heated capillary at 300 °C and an ion funnel RF level of 40%. The mass spectrometer was operated in a data-dependent mode, with an automatic switch between the MS and MS/MS scans using a top 12 method (minimum AGC target 8E3) and a dynamic exclusion time of 25 sec. MS (350-1500 m/z) and MS/MS

spectra were acquired with a resolution of 60,000 and 30,000 FWHM (200 m/z), respectively. Peptides were isolated using a 2 Th window and fragmented using higher-energy collisional dissociation (HCD) at 27% normalized collision energy. The ion target values were 3E6 for MS (25 ms maximum injection time) and 1E5 for MS/MS (54 ms maximum injection time). Two independent biological replicates and two technical replicates were analyzed.

The peptides contained in the unbound fraction were separated using a 90 min effective linear gradient (buffer A: 0.1% FA; buffer B: 100% ACN, 0.1% FA) at a flow rate of 250 nL/min. The gradient used was: 0-5 min 4% B, 5-7.5 min 6% B, 7.5-80 min 25% B, 80-94 min 42.5% B, 94-99 min 98% B, 99-105 min 2% B. The peptides were electrosprayed (1.9 kV) into the mass spectrometer through a heated capillary at 300 °C and an ion funnel RF level of 40%. The mass spectrometer was operated in a data-dependent mode, with an automatic switch between the MS and MS/MS scans using a top 12 method (minimum AGC target 8E3) and a dynamic exclusion time of 40 sec. MS (350-1500 m/z) and MS/MS spectra were acquired with a resolution of 60,000 and 15,000 FWHM (200 m/z), respectively. Peptides were isolated using a 2 Th window and fragmented using higher-energy collisional dissociation (HCD) at 27% normalized collision energy. The ion target values were 3E6 for MS (25 ms maximum injection time) and 1E5 for MS/MS (22 ms maximum injection time). Samples were analyzed twice.

Data analysis

Raw files from both K-ε-GG–enriched fraction and full proteome (flow-through, unbound fraction) were processed with MaxQuant (version 1.6.0.16) using the standard settings against a *Saccharomyces cerevisiae* protein database (UniProtKB/Swiss-Prot, 6,718 sequences) supplemented with contaminants. Label-free quantification was done with match between runs (match window of 0.7 min and alignment window of 20 min). Carbamidomethylation of cysteines was set as a fixed modification whereas addition of glycine-glycine to lysine (only for K-ε-GG–enriched fraction), methionine oxidation and N-term acetylation were variable protein modifications. The minimal peptide length was set to 7 amino acids and a maximum of two tryptic missed-cleavages were allowed. The results were filtered at 0.01 FDR (peptide and protein level) and subsequently the “proteinGroup.txt” file and the “GlyGly (K) Sites.txt” were loaded in Perseus (v1.6.0.7) for further statistical analysis. The intensity of the K-ε-GG–enriched fraction was

normalized by subtracting the median. A minimum of 75% valid values per group was required for quantification. Missing values were imputed with Perseus from the observed normal distribution of intensities. Then, a two-sample Student's T-Test with a permutation-based FDR was performed. Proteins with a q-value<0.05 and log_2 ratio >0.5 or < -0.5 and K-ε-GG– peptides with a q-value<0.1 and log_2 ratio >1 or < -1 were considered as regulated. The mass spectrometry proteomics data have been deposited to the ProteomeXchange Consortium via the PRIDE partner repository with the dataset identifier PXD028669.

Ubiquitin and SUMO Pull downs

Ubiquitin and SUMO pull-downs were done under denaturing conditions using protein extracts from yeast cells carrying the *UBI* gene fused to a 7His-tag, expressed from a plasmid under the control of the *CUP1* promoter; or the *SMT3* gene fused to a 6His-Flag epitope integrated at its endogenous location. In the first case, cultures were grown in SC-URA medium containing $CuSO_4$ at 20 µM.

25 OD_{600} of exponentially growing cells (100 OD_{600} for SUMOyated Rpa190 PD) were spun at 3.000 rpm 2 minutes in 50 ml tubes. Cells were then washed in cold water and transferred to a 1.5 ml tube. 250 µl of Buffer A (6 M Guanidine Chloride, 100 mM KH_2PO_4, 10 mM Tris-HCl, 0.05% Tween-20, 15 mM imidazole, 1X protease inhibitors; pH 8) and 500 µl of glass beads were added to the pellet. Cells were broken using a mini-beadbeater cell disrupter (BioSpec Products) at power 6 for 1,5 minutes. Next, we pierced the bottom of the tube with a 21 ga. needle and set it up over another 1.5 ml tube. After that, extracts were spun at 2.400 rpm to recover the cell extract and discard the beads. Following, we added 700 µl of Buffer A to the tube, mixed it and spun 10 minutes at 14.000 rpm at 4ºC. The supernatant was then transferred to a screw cap tube, and the volume brought up to 1 ml. Finally, we added 70 µl of Ni-NTA (Nickel Nitrilo-triacetic Acid) agarose beads (Qiagen), and incubated the mixture overnight at the orbital rotator at RT. Next, the tubes were spun at 3.400 rpm. The supernatant was transferred to a new tube, and the beads washed for 8 minutes with 900 µl of Buffer B (8 M urea, 100 mM KH_2PO_4, 10 mM Tris-HCl, 0.05% Tween-20, 2 mM imidazole; pH 8). Washes were repeated a total of three times with Buffer B and three times more with Buffer C (8 M urea, 100 mM KH_2PO_4, 10 mM Tris-

HCl, 0.05% Tween-20; pH 6.3). Finally, proteins bound to the beads were eluted with 25 µl of 2xSSR (4% SDS, 250 mM Tris-HCl pH 6.8, 10% sucrose, 0.02% bromophenol blue) by boiling 3 minutes at 95ºC. 30 µl of supernatants were precipitated with the same volume of TCA 12% (trichloroacetic acid), washed 3 times with chilled acetone, resuspended by vortexing in 30 µl of Buffer C and incubated at 37ºC for 20 min. Then, protein extracts (PE) were boiled with 30 µl of 2xSSR. Finally, PE and PDs were centrifuged and loaded onto a SDS-PAGE for Western Blot analysis.

Western blot analysis

This protocol was used for analysing Pol30-protein levels and modifications by Western Blot. Briefly, 10 OD_{600} from an exponentially growing culture were collected by centrifugation 4 minutes at 4.000 rpm and 4ºC, after adding 250 µl of TCA 20% directly to the culture. The pellet was resuspended with 500 µl of TCA 20%, transferred to a 1.5 ml tube and spun 6-7 seconds at high speed. Then, the supernatant was removed and the pellet was resuspended again with 100 µl of TCA 20%. After that, we added 500 µl of glass beads and broke cells in a mini-beadbeater cell disrupter (BioSpec Products) for 45 seconds. Next, the sample was transferred to a new tube by making a hole with a needle at the bottom and spinning 1 minute at 1.000 rpm. After that, we washed beads twice with 100 µl of TCA 5% and centrifuged 10 minutes at 3.000 rpm and RT. The supernatant was discarded and the pellet was resuspended with 100 µl of 1xSR (2% SDS in 0.125 M Tris-HCl pH 6.8) and neutralized with 50 µl of Tris-base 1 M. Samples were then boiled 3 minutes at 95ºC, centrifuged 5 minutes at 13.000 rpm and protein concentration was determined with the BIO-RAD Micro DC Protein Assay. Finally, 4xSS and β-Mercaptoethanol were added to a volume corresponding to 30 µg of protein, loaded onto an SDS-gel and analyzed by Western Blot.

Generation of *rpa190-KR* mutants

To obtain the *rpa190-K408,410R* allele, we mutagenized a plasmid expressing the wild type gene (*pRS314-(CEN-TRP1)-RPA190*) by PCR using a pair of primers containing the two point mutations and a PstI restriction site. Colonies were checked by PstI digestion and sequencing. The mutant and the wild type plasmids were then transformed into a diploid yeast strain with a deletion in one of the endogenous copies of *RPA190*. By

sporulation and tetrad dissection we isolated haploid yeast colonies carrying the *rpa190-K408,410R* plasmid and a deleted chromosomal *RPA190* copy. Next, we tagged the plasmid express copy with a 6HA tag and recovered the vectors from their yeast to obtain the *pRS314-(CEN-TRP1)-RPA190-6HA:natNT2* and *pRS314-(CEN-TRP1)-rpa190-K408,410R*-6HA:natNT2 plasmids. To integrate the double *KR* mutation into yeast, we used the mutant vectors as PCR templates. The PCR product was transformed into yeast and colonies carrying the desired mutation were selected by PstI restriction and sequencing.

Gene tagging

Gene tagging was performed following the protocol described by Janke *et al.,* (Janke *et al*, 2004), using a PCR-based method for recombinational integration. A set of cassette plasmids carrying a selectable marker and an epitope tag were amplified by PCR using the adequate primers to direct the insertion of the cassette to the desired locus by homologous recombination.

Yeast growth test analysis

10-fold dilution series of yeast cultures were spotted on solid medium. Plates were incubated at the adequate temperature during 2-3 days and photographed with the Chemiluminiscent Imager (Bio-Rad). For methyl methanesulfonate (MMS) growing test analysis, MMS was added from 0.001 to 0.02% final concentrations in the YPD agar media before solidification. BMH-21 (Sigma) was added to the YPD agar at a 15 µM concentration. Plates were incubated at 30°C until individual colonies became visible in control plates.

AKNOWLEDGEMENTS

The work in JT-R lab was supported by grants BFU2015-71308-P and PGC2018-097796-B-I00 from the Ministerio de Ciencia, Innovación y Universidades, and grant 2017-SGR-569 from AGAUR-Generalitat de Catalunya; the IRBLLEIDA institute is part of the CERCA Programme/Generalitat de Catalunya. The CNIO Proteomics Unit belongs to ProteoRed, PRB3- ISCIII, supported by grant PT17/0019/0005. Eva Ibars was supported by a PhD fellowship from UdL and 'Ajuts al talent en investigació Biomèdica' contract from

IRBLLEIDA and Diputació de Lleida. We thank Farida Dakterzada for construction of yeast strains, Herbert Tschochner for the pRS314-RPA190 plasmid, and Carlos Fernéndez-Tornero and all members of the Cell Cycle lab for helpful discussions.